



HAL
open science

Synthesis and properties of novel pyranilidene-based organic sensitizers for dye-sensitized solar cells

S. Gauthier, F. Robin-Le Guen, Laurianne Wojcik, Nicolas Le Poul, A. Planchat, Y. Pellegrin, P.G. Level, N. Szuwarski, M. Boujtita, D. Jacquemin, et al.

► To cite this version:

S. Gauthier, F. Robin-Le Guen, Laurianne Wojcik, Nicolas Le Poul, A. Planchat, et al.. Synthesis and properties of novel pyranilidene-based organic sensitizers for dye-sensitized solar cells. *Dyes and Pigments*, 2019, 171, pp.107747. 10.1016/j.dyepig.2019.107747 . hal-02281770

HAL Id: hal-02281770

<https://univ-rennes.hal.science/hal-02281770>

Submitted on 27 Nov 2020

HAL is a multi-disciplinary open access archive for the deposit and dissemination of scientific research documents, whether they are published or not. The documents may come from teaching and research institutions in France or abroad, or from public or private research centers.

L'archive ouverte pluridisciplinaire **HAL**, est destinée au dépôt et à la diffusion de documents scientifiques de niveau recherche, publiés ou non, émanant des établissements d'enseignement et de recherche français ou étrangers, des laboratoires publics ou privés.

Synthesis and properties of novel pyranylidene-based organic sensitizers for dye-sensitized solar cells

Sébastien Gauthier,^{a,*} Françoise Robin-Le Guen,^a Laurianne Wojcik,^b Nicolas Le Poul,^b

Aurélien Planchat,^c Yann Pellegrin,^{c*} Patricia Guevara Level,^c Nadine Szuwarski,^c

Mohammed Boujtita,^c Denis Jacquemin^{c,*} and Fabrice Odobel^{c,*}

^a Univ. Rennes, CNRS, ISCR (Institut des Sciences Chimiques de Rennes) - UMR 6226, F-35000 Rennes, France. E-mail: Sebastien.Gauthier@univ-rennes1.fr, Tel:+33 2 96 46 93 44.

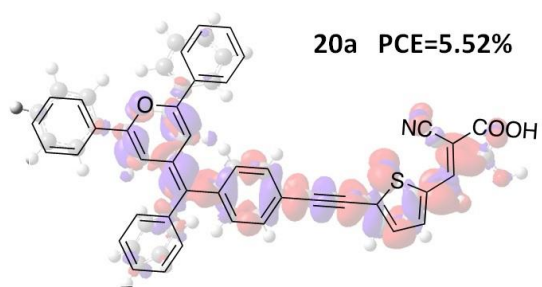
^b Laboratoire de Chimie, Électrochimie Moléculaires et Chimie Analytique, UMR CNRS 6521, Université de Bretagne Occidentale, UFR Sciences et Techniques, 6 avenue Victor Le Gorgeu – CS 93837, F-29238 Brest Cedex 3, France.

^c Université de Nantes, CNRS, Chimie et Interdisciplinarité: Synthèse, Analyse, Modélisation (CEISAM), UMR 6230, 2 rue de la Houssinière, 44322 Nantes Cedex 3, France. E-mail: Yann.Pellegrin@univ-nantes.fr, Tel +33 2 76 64 51 74; E-mail: Denis.Jacquemin@univ-nantes.fr, Tel: +33 2 51 12 55 67, E-mail: Fabrice.Odobel@univ-nantes.fr; Tel: +33 2 51 12 54 29.

Keywords

- Dye-sensitized solar cells
- Organic sensitizers
- Substituent effect
- Photovoltaic performance
- TD-DFT

Graphical abstract



Abstract

We report herein the synthesis of nine new molecularly engineered metal-free organic pyranilidene-based dyes as efficient photosensitizers for Dye-Sensitized Solar Cells (DSSCs). Their photophysical, electrochemical, and photovoltaic properties were investigated, and their excited states have been modelled using Time-Dependent Density Functional Theory (TD-DFT). The investigation of the photovoltaic performances of this series of new dyes provided structure-property relationships where their Power Conversion Efficiencies (PCE) could be correlated to structural features, such as the length of the π -conjugated spacer and the nature of the substituents on the upper (positions 2 and 6) and lower parts (substituents on the exocyclic carbon) of the pyranilidene electron donor moiety. While these dyes fulfilled the criteria of efficient sensitizers for TiO₂-based DSSCs, their photovoltaic performances were found to depend on the dye packing arrangements controlled by substituents on the pyranilidene group. The highest Power Conversion Efficiency of 5.52% was reached with the **20a** dye containing phenyl substituent groups in both upper and lower parts of the pyranilidene fragment and with one thienyl π -conjugated spacer.

1. Introduction

The increasing demand for energy along with the numerous environmental pollution issues resulting from burning fossil fuel have triggered the expansion of research into clean, affordable and renewable energy sources to accommodate and maintain the needs for a modern life-style of a growing worldwide population [1]. In this respect, sunlight is one of the most widely available natural renewable energy sources that can globally contribute to resolving the environmental and energy issues of the present century [2]. Over the past thirty years, several types of solar cells capable of efficiently harvesting the incident sunlight have been developed [3]. Currently, traditional silicon-based solar cells involving long energy payback time still dominate the photovoltaic market. However, new solar cell technologies based on thin films have emerged as promising efficient substitutes [4].

As alternatives to silicon-based solar cells, Dye-Sensitized Solar Cells (DSSCs) embody a new generation of photovoltaic devices exhibiting high potential in solar power conversion efficiency (PCE) [5]. DSSCs are easy to fabricate, colorful, transparent and more importantly they work well in low light conditions [5a, 6]. A typical DSSC is made of a photoanode consisting of a crystalline mesoporous semiconductor (n-type TiO_2) on which sensitizer dye molecules are adsorbed, an electrolyte acting as redox mediator (I^-/I_3^-), and a counter electrode (Pt). Among these components, the sensitizer dye is the key element defining the efficiency and the lifetime of the solar cell since it captures the sun light and initiates the electron transfer. Conventionally, transition metal complexes typically based on ruthenium and osmium metals have been used as efficient sensitizers with remarkable Power Conversion Efficiency (PCE) exceeding 10% [7].

However, these transition metals are on the verge of disappearing due to their limited natural availability combined with extensive recent uses. Consequently, they have become quite expensive, making them inappropriate for the development of cost-effective and environmentally friendly photovoltaic devices. Therefore, low-cost copper and zinc complexes have been investigated as DSSC dyes [8]. While such complexes exhibit good conversion efficiency comparable to those of ruthenium complexes, their practical applications in actual devices are hampered by their complicated and low-yield syntheses.

To circumvent the issues associated with transition metal complexes, metal-free organic dye sensitizers, usually based on a donor-(π -linker)-acceptor type push-pull molecules have attracted considerable attention due to their simple and affordable synthetic process, their tunable structure, their high molar extinction coefficient, and their excellent intramolecular charge transfer (ICT) properties [9]. Numerous metal-free organic dyes have been investigated, and some have been found to exhibit conversion efficiency performances similar to those displayed by ruthenium-based complexes [10]. Various chromophores containing conjugated electron donor groups, such as triphenylamine [11], dialkylaminophenyl [12], indoline [13], carbazole [14], dithiafulvene [15] and tetrathiafulvalene (TTF) [16] groups have been investigated. While a variety of π -linkers have been incorporated into these organic dyes to foster the ICT and improve the light-harvesting ability, cyanoacrylic acid remains the most popular due to its dual role as electron acceptor group (cyano) and an anchoring (carboxylic acid) moiety, resulting in excellent electron injection properties on titanium oxide [17].

γ -Pyranlydene fragments are pro-aromatic electron-donating groups widely developed by Garín et al. [18] and our group [19]. Their electron-donating ability is based on the formation of an aromatic pyrylium fragment resulting from an intramolecular charge transfer process. In previous studies, the γ -pyranlydene moiety has been incorporated as an electron-donating group in various platinum- and ruthenium-based organometallic complexes and organic molecules for the preparation of push–pull structures with large second-order Non-Linear Optical (NLO) properties [20] or valuable behavior in DSSCs [21]. Pyranlydenes are easily synthesized molecules and they can be directly modified by the addition of different substituents in the 2 and 6 or on the exocyclic carbon, which allows to incorporate them as electron donor groups in push-pull chromophores. Very recently, the modification and optimization of pyranlydene derivatives, investigated as sensitizers for DSSCs, have led to encouraging Power Conversion Efficiency results reaching up to 6% [22].

Herein, we present nine new push-pull organic dyes **10b-d**, **12a-b**, **19a**, **20a**, **21a** and **22a** (Chart) based on the pyranlydene group as push (electron donor) unit. Our goal was to investigate the structure-property relationships within this class of dyes. The compound **20a** was taken as reference. First, we studied the impact of the length of the thienyl π -conjugated spacer (Chart Parameter I) on the photovoltaic properties (comparing **20a** to both **21a** and **22a**). Then we evaluated how the nature of the substituents on the upper part (positions 2 and 6, Chart Parameter II) or on the lower part (substituents on the exocyclic carbon, Chart Parameter III) of the pyranlydene moiety affects these properties by comparing **20a** to **10b** to **10c** to **10d**, and **20a** to **12a** to **12b** to **19a**, respectively.

In this paper, we describe the syntheses, characterizations, electronic properties and theoretical investigations of this series of new dyes. The measurements of the photovoltaic performances in TiO₂-based DSSCs, coupled with Intensity-Modulated Photovoltage

Spectroscopy (IMVS) experiments enable us to establish structure-property relationships for these dyes by correlating the changes of their efficiencies to their structural modifications, and to show that the photovoltaic performances are predominantly controlled by the π -conjugated spacer as well as by the substituents placed on the exocyclic carbon on the pyranilidene electron donor.

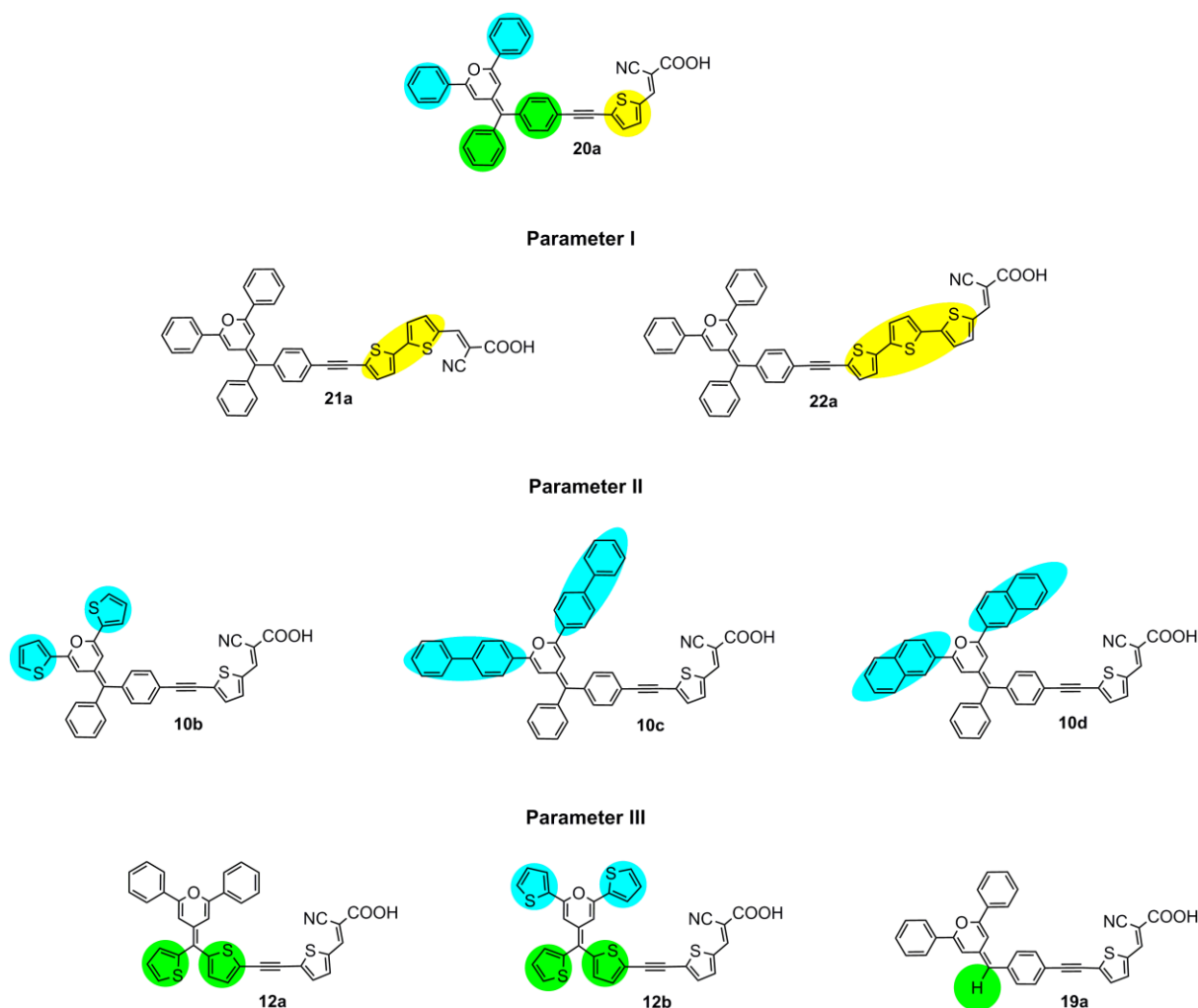
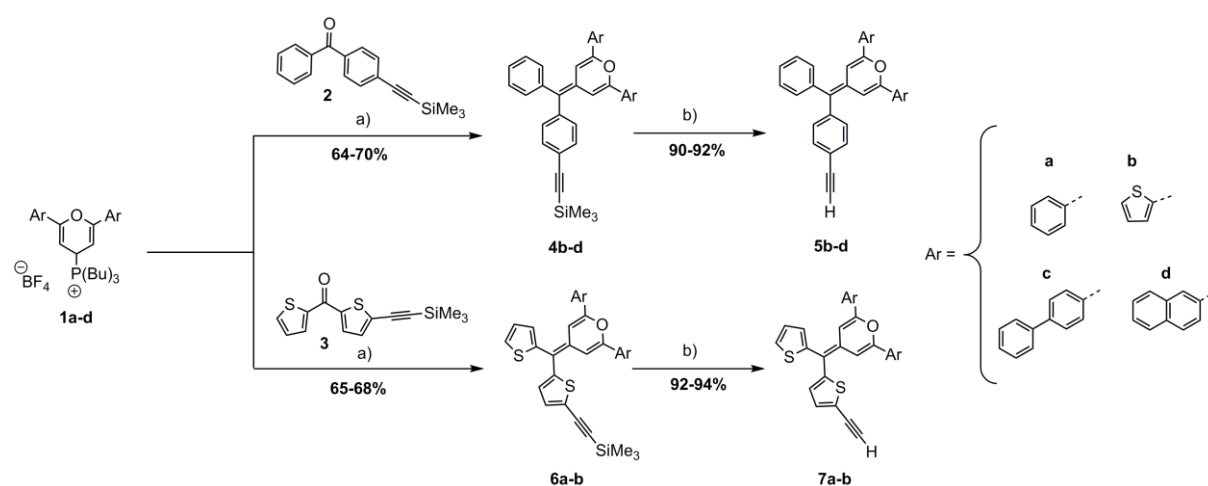


Chart. Structures of the dyes investigated in this work. The dye **20a** has been drawn as reference to show the moieties corresponding to the investigated parameters within each series (highlighted in yellow, blue and green).

2. Results and Discussion

2.1. Synthesis of the Dyes

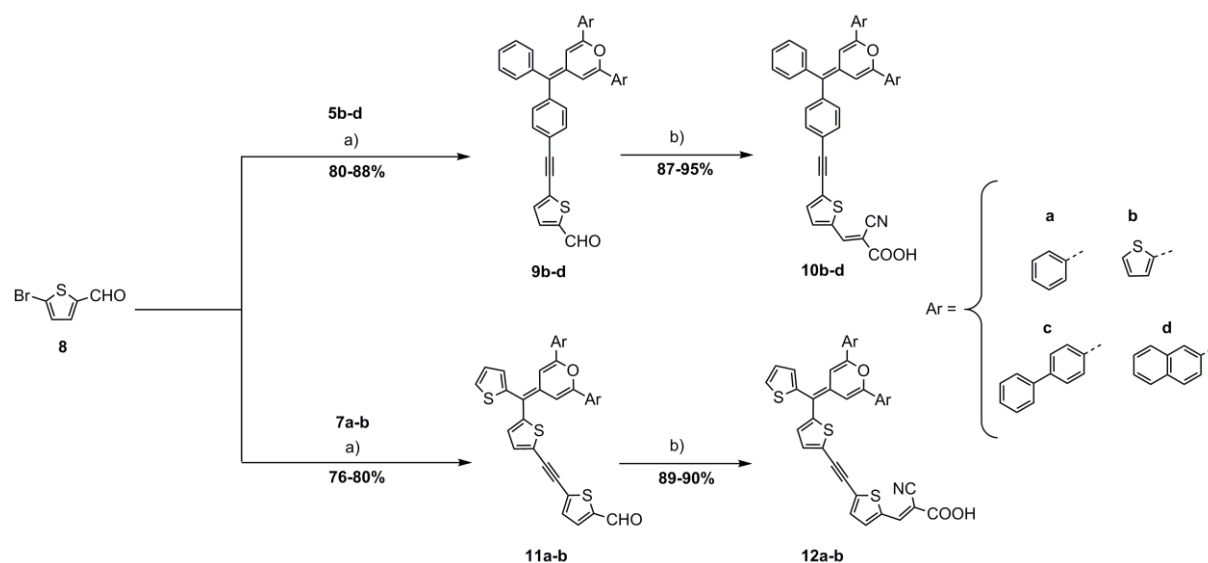
The key intermediate for obtaining the push-pull dyes is the alkynes **5b-d**, **7a-b**, **13a**, and **14a** (see Schemes 1-3). First, the two alkynes **13a** and **14a** are prepared following known synthetic routes [19c, 21a]. Identical synthetic methods have been used for **5b-d** and **7a-b**, which are obtained in two steps from 4-(2-trimethylsilylethynyl)benzophenone **2** or 5-(2-trimethylsilylethynyl)thienone **3** and the desired phosphonium tetrafluoroborate salt **1a-d** (Scheme 1). The syntheses of the precursors **1a-d** and **2** are described in supporting information. The first step is a Wittig reaction leading to the intermediates **4b-d** and **6a-b** in good yield and the second step consists of the deprotection of the trimethylsilyl group in quasi-quantitative yield.



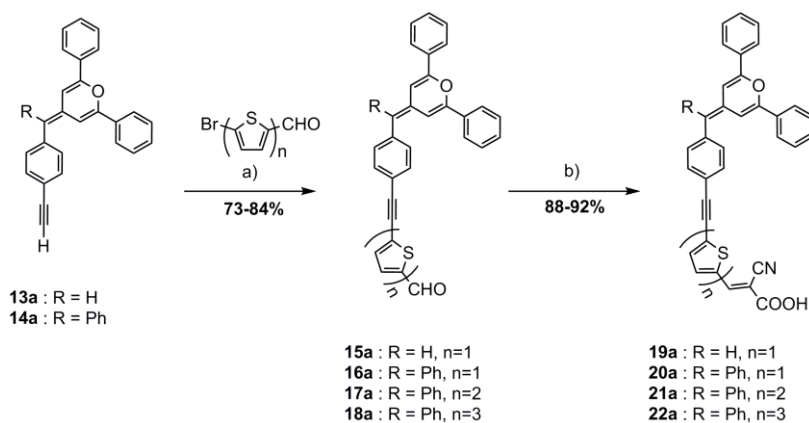
Scheme 1. Synthetic route of alkyne compounds **5b-d** and **7a-b**. Reagents and conditions : a) THF, *n*-BuLi, -78°C to r.t., 2h b) K₂CO₃, CH₂Cl₂/MeOH, r.t., overnight.

The carboxaldehyde intermediates **9b-d**, **11a-b**, **15a**, **16a**, **17a**, and **18a**, are then obtained *via* a copper/palladium catalyzed Sonogashira cross-coupling reaction between **5b-d** or **7a-b** and the corresponding aldehydes (Scheme 2 and 3). Finally, the dyes **10b-d**, **12a-b**, **19a**, **20a**, **21a**, and **22a** are obtained in good yields (80–95%) by Knoevenagel reactions of the corresponding

precursors with cyanoacetic acid in the presence of piperidine and subsequent acid wash (Schemes 2 and 3).



Scheme 2. Synthetic routes of dyes **10b-d** and **12a-b**. Reagents and conditions: a) Pd(PPh₃)₄, CuI, THF, NH*i*Pr₂, 60° C, overnight. b) Cyanoacetic acid, piperidine, CHCl₃, reflux, overnight.



Scheme 3. Synthetic route of dyes **19a**, **20a**, **21a**, and **22a**. Reagents and conditions: a) Pd(PPh₃)₄, CuI, THF, NH*i*Pr₂, 60° C, overnight. b) Cyanoacetic acid, piperidine, CHCl₃, reflux, overnight.

All the target sensitizer dyes have been characterized by ¹H and ¹³C NMR, and high-resolution mass spectroscopy, see Supporting Information (SI). The prepared dyes are also perfectly stable in their solid state form and did not require any specific storage conditions.

2.2. Electronic UV-visible absorption

The electronic spectra of compounds **10b-d**, **12a-b**, **19a**, **20a**, **21a**, and **22a** recorded in dichloromethane solution (1.1×10^{-5} M) in the 300–800 nm wavelength range are displayed in Figure 1 and the positions of the bands are listed in Table 1. For all compounds, the least energetic absorption band in the visible region can be assigned to an ICT process between the donor and the acceptor moieties (see theoretical calculations below). The molar extinction coefficients (ϵ) of compounds **10b**, **12a**, **19a**, **20a**, **21a**, and **22a** exceed $20,000 \text{ M}^{-1}\text{cm}^{-1}$ with a maximum at $53,000 \text{ M}^{-1}\text{cm}^{-1}$ for compound **22a**. These coefficients exceed those of the standard ruthenium N3 [23] and N719 [24] dyes ($13,900$ and $14,000 \text{ M}^{-1}\text{cm}^{-1}$, respectively), indicating that most of the dyes of this series are good candidates for light harvesting. The UV-visible spectra also show that the modification of the aromatic fragment on the exocyclic carbon on **20a** (phenyl) and **12a** (thienyl) resulted in red-shifted ICT absorption bands. The groups placed in the 2- and the 6- positions of the pyranilidene fragment, i.e., phenyl, thienyl, naphthyl and biphenyl have a limited influence (10 nm) on the absorption spectra. The increase of the intensity (molar extinction coefficients) of the maximum absorption of **21a** and **22a**, as compared to that of **20a**, can be explained by the enhanced electron delocalization over the oligothiophene spacers of increasing length. Overall, among all the dyes, **12a** and **12b** demonstrate the broader absorption spectra, while **10d** and **10c** appear as being the poorest light collectors.

Table 1. Absorption properties of the dyes **10b-d**, **12a-b**, **19a**, **20a**, **21a**, and **22a** recorded in CH₂Cl₂ (1.1 × 10⁻⁵ M) at room temperature.

Dye	λ_{\max}/nm ($\epsilon \times 10^4 \text{ M}^{-1} \cdot \text{cm}^{-1}$)	$\lambda_{\text{onset}}/\text{nm}^a$
10b	389 (5.3), 472sh (3.0)	568
10c	391 (5.0), 488sh (2.4)	581
10d	396 (3.0), 490sh (1.0)	568
12a	399 (3.5), 530 (1.9)	653
12b	406 (3.4), 520 (2.3)	655
19a	387 (3.9), 462 (3.3)	574
20a	387 (4.8), 480sh (2.3)	568
21a	443 (3.9)	550
22a	365 (2.8), 469 (5.1)	558

^a Estimated from the wavelength with the intersections tangent method (λ_{onset}).

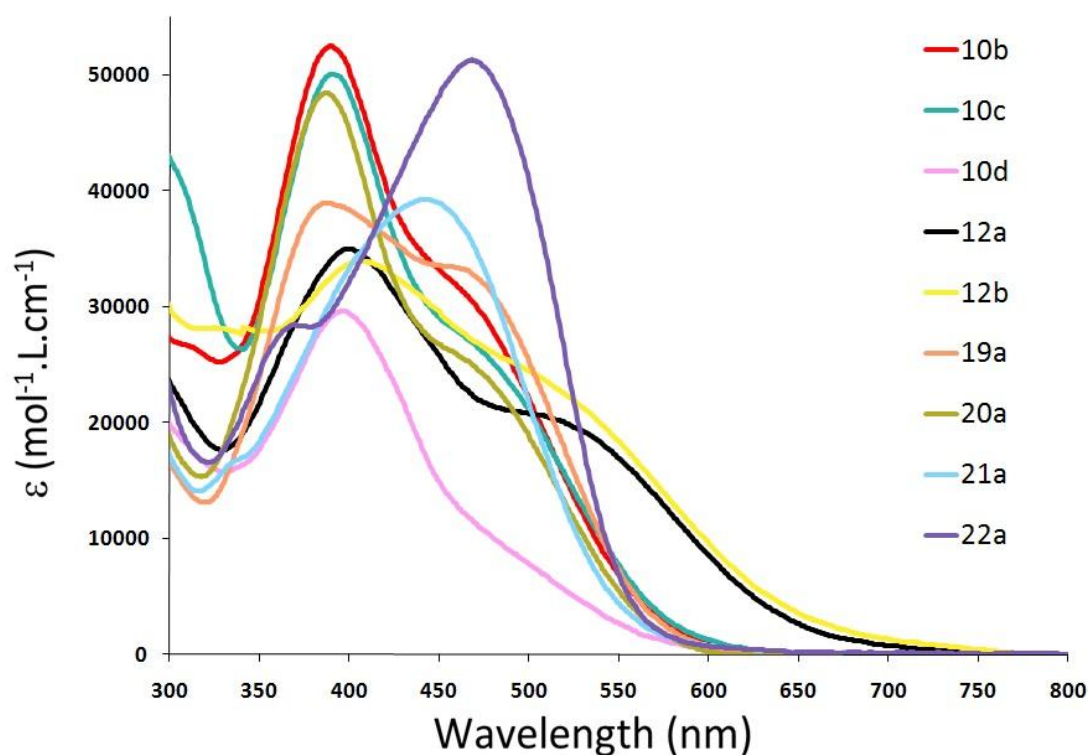


Figure 1. UV-Vis absorption spectra of dyes **10b-d**, **12a-b**, **19a**, **20a**, **21a**, and **22a** in CH₂Cl₂ solution (1.1 × 10⁻⁵ M) at room temperature.

2.3. Electrochemical study and electron transfer driving forces

The synthesized dyes were studied by cyclic voltammetry (CV) at a Pt working electrode in $\text{CH}_2\text{Cl}_2/\text{NBu}_4\text{PF}_6$ 0.1 M. The electrochemical data are gathered in Table 2. All dyes, except **19a**, display two successive oxidation processes, as previously observed with pyranilidene analogues [20a, 21a]. As shown in Figure 2 for compound **20a**, the first process at $E^0(1)$ is fully reversible at $\nu = 0.1 \text{ V s}^{-1}$ (Figure 2A, black curve) and is ascribed to the mono-oxidation of the pyranilidene moiety, leading to the formation of a pyrylium compound. The second process at $E^0(2)$ is quasi-reversible for all compounds excepted for **19a** and leads to the formation of an unidentified species which is reducible at *ca.* -0.1 V vs. NHE on the backscan (Figure 2A, red curve). Scanning towards negative potentials (Figure 2B) shows the presence of broad and irreversible peaks in the -0.4 V to -0.8 V potential range, corresponding to the reduction of the cyanoacrylic acid anchoring group [21a]. The specific redox behavior of compound **19a** is consistent with previous studies on H-pyranilidenes, which showed that the oxidation of the pyranilidene is followed by fast dimerization yielding bis-pyrylium species [25]. Such dimerization process does not occur when a substituent different than H (**19a**) is linked to the exocyclic carbon. Analysis of the data for the oxidation processes indicates that the nature of the phenyl or thienyl spacer has a significant effect on the redox properties. For example, the simple switch from a phenyl to a thienyl spacer in close position to the pyranilidene (**20a** to **12a**) decreases both $E^0(1)$ and $E^0(2)$ values by 60 mV and 200 mV, respectively (see Table 2). This effect probably results from an increase of the electron density delocalization, (see computational part below). Hence, compound **12b** displays the lowest $E^0(1)$ value amongst the investigated compounds. Moreover, as previously concluded for Pt complexes [21a], the increase of the chain length between the cyanoacrylic acid group and the phenyl-substituted pyranilidene moiety from one to three thienyl groups (compounds **20a**, **21a** and **22a**) does not induce any major changes on the voltammetric response, neither

in oxidation nor in reduction (Table 2). Finally, CV studies emphasize that groups in the 2,6 positions of the pyranilidene ring do not influence the redox behavior (compounds **20a**, **10b-d**).

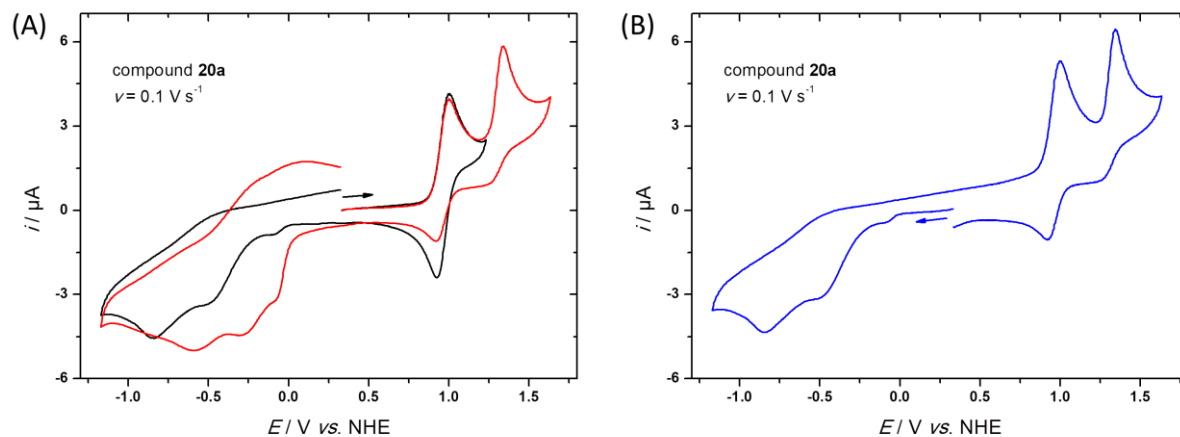


Figure 2. Cyclic voltammetry at a Pt electrode of compound **20a** in $\text{CH}_2\text{Cl}_2/\text{NBu}_4\text{PF}_6$ 0.1 M ($\nu = 0.1 \text{ V s}^{-1}$, $C = 0.5 \text{ mM}$); A) in positive initial scanning; B) in negative initial scanning. Experimental curves were measured against Fc and recalibrated by taking $E^0(\text{Fc}^+/\text{Fc}) = 0.71 \text{ V vs. NHE}$ in those conditions.

Table 2. Electrochemical data for **10b-d**, **12a-b**, **19a**, **20a**, **21a** and **22a** (0.5 mM) at a Pt working electrode in $\text{CH}_2\text{Cl}_2/\text{NBu}_4\text{PF}_6$ 0.1 M ($E / \text{V vs. NHE}^a$, $\nu = 0.1 \text{ V s}^{-1}$). ΔG_{inj} and ΔG_{reg} values for **10b-d**, **12a-b**, **19a**, **20a**, **21a** and **22a**.

Dye	$E^0(1)^a$	$E^0(2)^a$	$E_{\text{pc}}(3)^a$	$E_{\text{pc}}(4)^a$	$E(\text{S}^*/\text{S}^+)^b$	ΔG_{reg}^c	ΔG_{inj}^c
10b	0.98	1.24	^d	-0.65	-1.20	-0.63	-0.70
10c	0.95	1.28	-0.51	^d	-1.19	-0.60	-0.69
10d	0.97	1.29	-0.44	-0.83	-1.21	-0.62	-0.71
12a	0.91	1.10	-0.53	-0.78	-0.99	-0.56	-0.49
12b	0.90	1.08	-0.55	-0.79	-0.99	-0.55	-0.49
19a	1.02 ^e	^d	-0.39	-0.61	-1.14 ^f	-0.67 ^f	-0.64 ^f
20a	0.97	1.30	-0.47	-0.83	-1.21	-0.62	-0.71
21a	0.96	1.27	-0.47	-0.75	-1.29	-0.61	-0.69
22a	0.96	1.24	^d	-0.84	-1.26	-0.61	-0.76

^a Values calibrated vs. NHE from the experimental curves obtained vs. Fc^+/Fc , by taking $E^0(\text{Fc}^+/\text{Fc}) = 0.47 \text{ V vs. SCE}$ in $\text{CH}_2\text{Cl}_2/\text{NBu}_4\text{PF}_6$ (measured experimentally) and $E^0(\text{SCE}) = 0.24 \text{ V vs. NHE}$.

^b $E(\text{S}^*/\text{S}^+)$: Fermi level (in V vs NHE) of excited molecules, calculated from :

$E(\text{S}^*/\text{S}^+) = E^0(1) - E_{0-0}(\text{S}/\text{S}^*)$, where E_{0-0} is the stored excitation energy, obtained from λ_{onset} .

^c ΔG in eV, $\Delta G_{\text{reg}} = E^0(\text{I}/\text{I}_3^-) - E^0(1)$ with $E^0(\text{I}/\text{I}_3^-) = 0.35 \text{ V vs NHE}$; $\Delta G_{\text{inj}} = E(\text{S}^*/\text{S}^+) - E_{\text{CB}}(\text{TiO}_2)$ with $E_{\text{CB}}(\text{TiO}_2) = -0.5 \text{ V vs NHE}$.

^d Peak not detected.

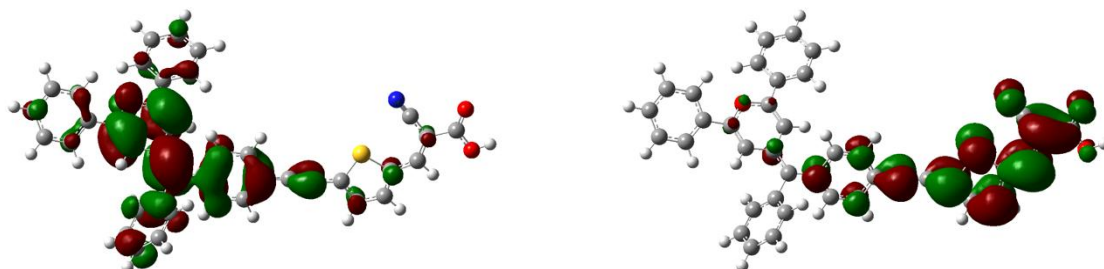
^e Irreversible anodic peak value.

^f Values estimated by assuming that $E^0(1) = (E_{pa}(1))$

The measured oxidation potentials were used to estimate the injection (ΔG_{inj}) and dye regeneration (ΔG_{reg}) free energies (Table 2). As these dyes are not luminescent, the 0-0 energy (E_{0-0}) was estimated from λ_{onset} of the absorption spectra. The results of Table 2 clearly indicate that all the dyes display very significant Gibbs free energies, which is more than sufficient to obtain efficient electron injection in the conduction band of TiO_2 ($\Delta G_{inj} \approx -0.5$ to -0.8 eV) and to oxidize iodide into triiodide ($\Delta G_{reg} \approx -0.6$ eV) (Table 2). In fact, these values are quite constant within this series of dyes, suggesting that the photovoltaic performances will not likely be controlled by these energetic parameters. Accordingly, ΔG_{reg} and ΔG_{inj} values are slightly over-estimated for **19a**, because $E^0(1)$ corresponds to an anodic peak potential, not a half-wave potential, due to the irreversibility of the oxidation process for this dye.

2.4. Quantum chemical calculations

To gain more insights into the nature of the electronic excited states, we performed Time-Dependent Density Functional Theory Calculations on all dyes, with an approach taking into account solvation effects (CH_2Cl_2) and detailed in the SI together with all HOMO and LUMO plots and energies. One representative example is given on Figure 3.



HOMO

LUMO

Figure 3. Contour plots of the HOMO and -LUMO orbitals of dye **20a**.

As illustrated in Figure 3, the HOMOs are systematically centered on the pyranilidene segment, whereas the LUMO is located on the cyanoacrylic moiety and vicinal thienyl ring. This represents a very favorable configuration for the efficient injection of electrons in the TiO₂ conduction band, since, upon light absorption, the electron density undergoes a significant shift from one extremity of the molecule to the other one at the site of the anchoring group. More quantitatively, the computed lowest dipole-allowed transitions are listed in Table 3 together with the ICT parameters as obtained by the so-called Le Bahers' d_{CT} approach [26, 27].

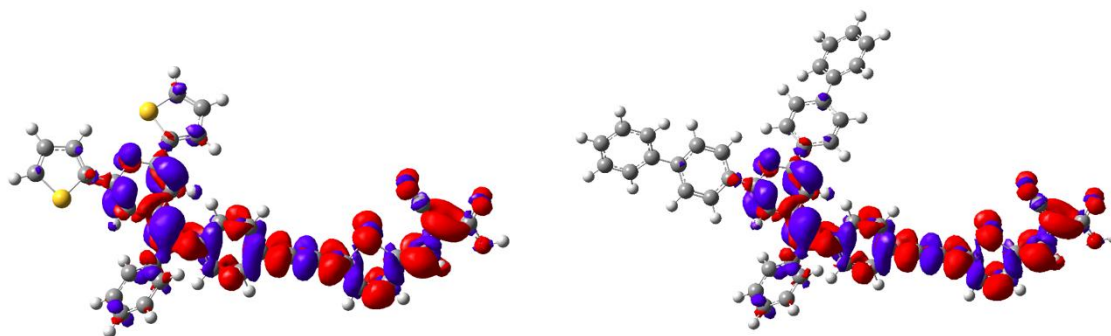
Although TD-DFT vertical transition energies do not strictly correspond to the absolute experimental λ_{max} , we note a good qualitative match between the computed values (Table 3) and the measured ones (Table 1), with, in particular: i) almost no change of the absorption band positions within a series of homologous dyes (**10b**, **10c**, **10d** and **12a**, **12b**); ii) a significant bathochromic shift when going from **10** to **12** (computed value: ca. +60 nm, measured value: ca. +40 nm), which can be explained by the more delocalized nature of the HOMO in the latter compounds (see SI); and iii) **19a-22a** transition energies quite similar to those of **10b-10d**. In addition, the energies of the frontier MOs are not strongly affected by the substitutions on the pyranilidene moiety (see SI), consistently with the electrochemical study described above. The data listed in table 3 show that the ICT parameters are large for all dyes at the exception of the dyes **12a**, **12b**, and **22a**, due to the absorption of light inducing a charge transfer of ca. 0.6-0.7 electron over more than 5 Å.

This ICT is illustrated in Figure 4 with the electron density difference plots clearly showing strong variations of the densities. The cyanoacrylic moiety, mostly in red, exhibits the characteristic electron density of an acceptor and the pyranilidene group, mostly in blue, that

of a donor, whereas the side rings of the donor do not play any significant role in the charge transfer. In both **12a** and **12b**, the addition of thienyl groups on the exocyclic carbon on the pyranilydene group results in an increased electron density delocalization, inducing absorption redshifts. However, the theory shows that, as a consequence of this delocalization, a smaller ICT is obtained, probably due to the diffuse nature of the HOMO (*vide supra* see SI). For **22a**, the data in table 3 also show a less effective ICT, which is clearly explainable from the plots of Figure 4: in this dye, the donating and accepting moieties are so far apart that the charge transfer actually occurs from the π -linker to the accepting moiety, the donor playing almost no role in the lowest electronic transition. This illustrates the well-known fact that longer linkers do not necessarily yield strong CT [28].

Table 3. Theoretical vertical excitation wavelength [PCM-CAM-B3LYP/6-311+G(2d,p)] in nm, oscillator strength (between brackets), together with the CT parameters of all dyes: d_{CT} and q_{CT} given respectively in Å and in e.

Dye	λ^{vert}/nm	$d_{CT}/\text{Å}$	q_{CT}/e
10b	485 (1.6)	5.44	0.73
10c	485 (1.7)	5.42	0.75
10d	485 (1.7)	5.40	0.73
12a	547 (1.4)	4.49	0.67
12b	554 (1.4)	4.55	0.68
19a	489 (2.0)	5.33	0.68
20a	480 (1.6)	5.50	0.75
21a	485 (2.3)	5.29	0.63
22a	495 (2.4)	4.56	0.58



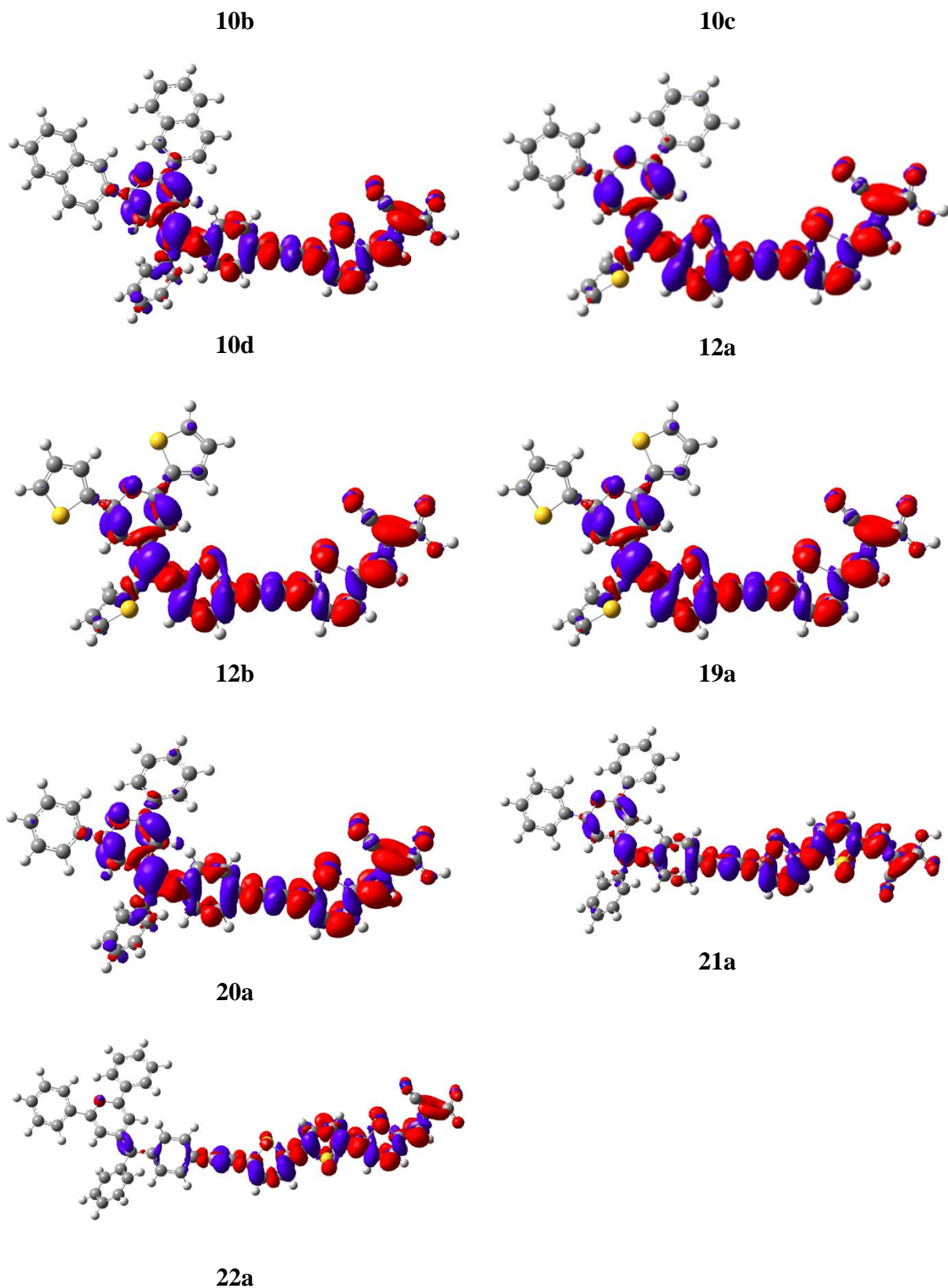


Figure 4. EDD plots obtained for all dyes. The blue (red) lobes represent regions of density decrease (increase) upon excitation, that is donor (acceptor) regions. Contour threshold: 0.0008 au.

2.5. Photovoltaic measurements and Intensity-Modulated Photovoltage Spectroscopy (IMVS) experiments

The synthesized push-pull dyes were used to prepare dye sensitized solar cells made of one layer of nanocrystalline TiO₂ particles (12 μm thick) and one layer of scattering TiO₂ particles (4 μm thick) and containing an iodide/triiodide-based electrolyte (see experimental part for details). The naked electrodes were dyed overnight at room temperature in a tertbutanol/acetonitrile solvent mixture. All the cells were also studied by IMVS in order to determine the electron lifetime (τ_{e^-}) for each dye. The electron lifetime (τ_{e^-}) corresponds to the average time that the injected electrons in TiO₂ last before charge recombination either with the oxidized dye or with triiodide redox mediator in the electrolyte takes place.

It is well known that organic dyes tend to aggregate after their chemisorption on TiO₂ surface. This process induces an excited state quenching and is therefore detrimental to the electron injection efficiency [29]. Accordingly, we first investigated the impact of the increasing concentration of chenodeoxycholic acid (CDCA) in the dye bath for chemisorption of dye **20b** and found that the optimal concentration was 1 mM (Table S1). Indeed, in absence of CDCA the aggregation adversely impacts the performances of the solar cell, but, since CDCA is a competitor to the dye adsorption a large concentration of CDCA decreases the dye loading and consequently the short-circuit current (J_{sc}). These optimal chemisorption conditions (dye at 0.25 mM in CH₂Cl₂/EtOH:1/1 with 1 mM of CDCA) and electrolyte composition ([tBuPy] = 0.1 M) were used to determine the photovoltaic performances of the entire series of dyes. The UV-Vis spectra of the photoanodes are given in the SI (Figure S60), and show that all electrodes strongly absorb light in the visible and thus display more than 90% light harvesting efficiency until 550 nm. Moreover, **12a** and **12b** dyed photoanodes exhibit particularly red-shifted absorption, in agreement with their absorption spectra recorded in solution. The metrics of the solar cells compiled in Table 4 are the average of at least 6 cells made with the

same dye. The incident photon-to-current efficiency (IPCE) spectra of the solar cells are shown in Figure 5.

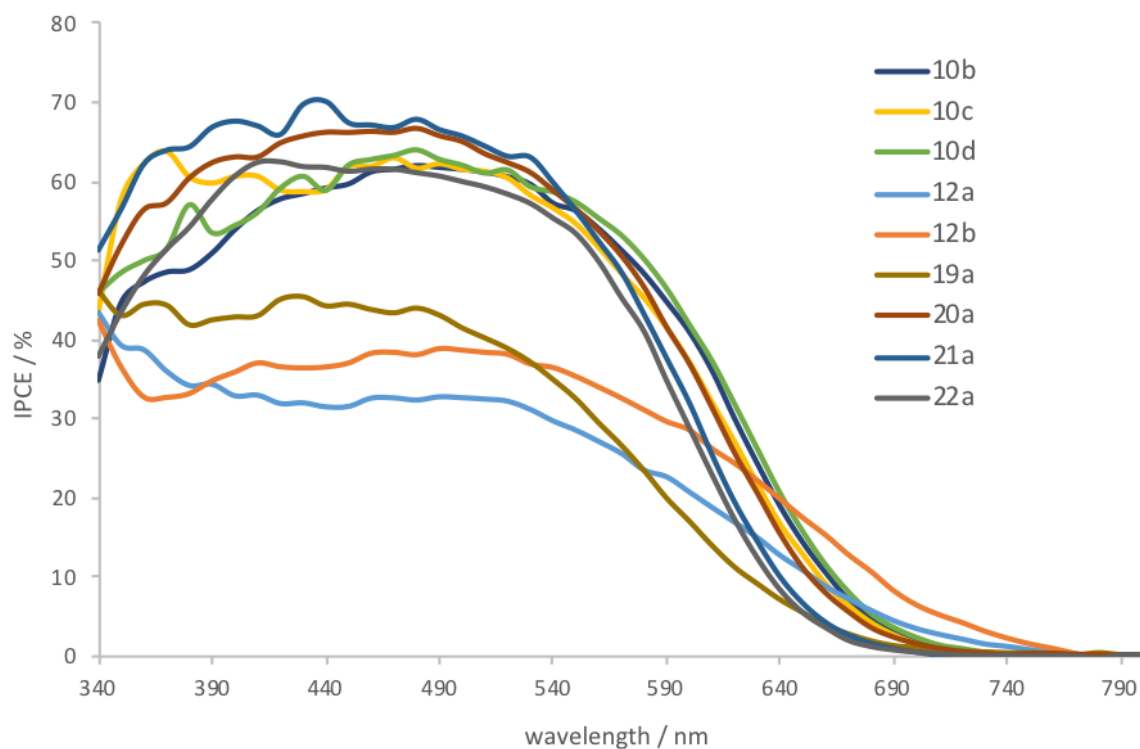


Figure 5. IPCE spectra of the dyes.

Table 4. Metrics of the solar cells fabricated illuminated with a calibrated sunlight AM1.5 (100 mW/cm²). The electron lifetime was measured by IMVS at a power of 150W/m².

Dye	J _{sc} (mA/cm ²)	V _{oc} (mV)	FF (%)	PCE (%)	Electron Lifetime (ms)
10b	10.8 (±0.1)	588 (±4)	70 (±1)	4.44 (±0.03)	24.19
10c	12.9 (±0.2)	605 (±1)	70 (±1)	5.41 (±0.09)	23.96
10d	11.9 (±0.2)	594(±1)	71(±1)	5.05 (±0.10)	29.47
12a	4.6 (±0.1)	481 (±5)	66 (±1)	1.47 (±0.11)	14.23
12b	6.7 (±0.1)	505 (±1)	68 (±1)	2.31 (±0.05)	13.70
19a	7.3 (±0.3)	480 (±2)	63 (±1)	2.19 (±0.10)	25.50
20a	13.1 (±0.1)	603 (±1)	70 (±1)	5.52 (±0.01)	43.67
21a	10.5 (±0.2)	590 (±1)	72 (±1)	4.44 (±0.08)	44.29
22a	11.1 (±0.3)	566 (±2)	70 (±1)	4.41 (±0.09)	17.62

Overall, the best performing dyes are **20a** and **10c**, while the least efficient ones are **12a**, **12b** and **19a**. The dyes **12a** and **12b** were found to show a less effective CT than most dyes investigated, whereas **20a** and **10c** showed amongst the strongest CT character (Table 3). In this series of dyes, there is almost no correlation between the Light Harvesting Efficiency (LHE) (broad and intense absorption spectra) and the J_{sc} delivered by the sensitizers. However, it is worth noting that the small d_{CT} estimated by TD-DFT in the case of **12a** and **12b** correlates well with the quite low J_{sc} measured for those two dyes.

Conversely, the most efficient dyes are characterized by the longest electron lifetime in TiO_2 , meaning that this parameter is the major key player for the efficiency. Below, we discuss the influence of the dye structural modifications (parameters), as described on the chart given in the introduction, on their photovoltaic performances.

The first parameter is the length of the spacer (i.e. the number of the thienyl units in the π -conjugated spacer), which connects the pyranilidene moiety to the anchoring cyanoacrylic acid group (**20a** versus **21a** versus **22a**). Although the Light Harvesting Efficiency (LHE) increases, as expected, with the number of thienyl units (Figure 2 and table 1), since the enhanced π -conjugation decreases the energy gap between the HOMO and LUMO, and consequently, red-shifts the absorption bands (Figures 1 and S58) but without improving the CT character (*vide supra*), the Power Conversion Efficiency (PCE) steadily decreases when the spacer length increases, due to a decrease of both J_{sc} and V_{oc} .

These results point to an increase of the charge recombination process, which is known to reduce both the charge collection efficiency and the concentration of electrons in the conduction band and thereby the V_{oc} . Upon inspection, the electron lifetime of these three dyes (**20a**, **21a** and **22a**) in TiO_2 can be ranked as follows: **20a** \approx **21a** > **22a**, which is consistent with the photovoltaic results of these three molecules. Indeed, when the electron lifetime increases, the V_{oc} improves (Figure S59). Logically and assuming a dye standing

upright, when the length of the spacer increases, the distance between the hole on the dye and the electron in TiO₂ should increase and consequently the charge recombination should diminish. However, the opposite result is obtained with the dyes **20a**, **21a** and **22a** for which an increase of the spacer length leads to an increase of the charge recombination process. As shown in table 3, the calculated d_{CT} for these dyes decreases when the length of the linker increases, which is in agreement with a lower injection efficiency. However, it is also possible that the **20a**, **21a** and **22a** dyes are bent on the TiO₂ surface. Since the oligothiophene is not a linear molecule, these dyes may not be able to stand perpendicular to the TiO₂ surface, thus resulting in a distance between the hole on the dye and the TiO₂ surface being similar for all three dyes. Conversely, the dye loading for **20a** is significantly smaller than those of **21a** and **22a** (table S3) indicating that those dyes could be more aggregated at the surface of TiO₂ than the **20a** dye, thus resulting in smaller Voc and Jsc values.

The second parameter investigated was the influence of the nature of the substituents in the 2 and 6 positions of the pyranilidene moiety on the photovoltaic properties of the **20a**, **10b**, **10c** and **10d** dyes. Within this series of dyes, the nature of these substituents does not seem to significantly alter the electronic properties of the dyes, since the redox potentials (Table 2), the absorption spectra (Figure 1 and Table 1) and the CT character (Table 3) of these dyes (**20a**, **10b**, **10c** and **10d**) are all quite similar. This is consistent with the topology of the HOMO and LUMO that almost do not involve these substituents (Figure S59). Unsurprisingly, the photovoltaic performances of all these dyes are also quite similar, at the exception of the dye **10b** containing thienyl groups as 2 and 6 substituents and displaying a significantly lower PCE (see **20a versus 10b**) due to a lower Jsc and Voc. These results can be explained by a lower electron lifetime in TiO₂ (Figure S61) observed for **10b** compared to those observed for **20a**. Since both dyes exhibit similar electronic properties and similar loading capacities (table S3), we infer that the thienyl groups (whose affinity for iodine has

been reported) [30] tend to increase the local I_3^- concentration and thus favor interfacial charge recombination. This is in line with the lower V_{oc} observed for 10b-based devices.

Finally, the influence of the nature of the substituents placed on the lower part of the pyranilidene moiety (substituents on the exocyclic carbon) on the photovoltaic performances of **20a**, **12a**, **19a**, **12b** and **10b** dyes was examined. For those substituents, the replacement of a phenyl by a thienyl (**20a** versus **12a** or **10b** versus **12b**) naturally leads to a red shift of the absorption band, but the J_{sc} of the DSSC made with **12a** is lower than that made with **20a** (the same observation can be made when comparing **10b** to **12b**), indicating that either electron injection quantum yield or charge recombination come into play. The Gibbs free energy of the electron injection of this series of dyes is ranked according to the same order than their J_{sc} values (**20a** > **19a** > **12a** \approx **12b**) suggesting that the differences of J_{sc} could be partly related to the driving forces (Table 2). In addition, the V_{oc} values follow the same trend in relation with the electron lifetime in TiO_2 , implying that charge recombination processes also significantly control the J_{sc} and the V_{oc} values (Figure S63). Interestingly, the dye loading for **19a** and **12a** is drastically higher than that of **20a**, and it could be once again inferred that **19a** and **12a** are more prone to aggregate, leading to overall poor photoconversion efficiencies as well as very poor V_{oc} and lower J_{sc} values. As mentioned above, however, the thienyl groups can contribute to increase the I_3^- concentration close to TiO_2 and this will also lead to low V_{oc} . Overall, the replacement of the phenyl substituents on the lower part of the pyranilidene or their substitution on the upper part by a thienyl seems to negatively impact the organization of the dyes on the TiO_2 surface, and consequently increases the charge recombination, as demonstrated by the decreasing electron lifetime measurements.

3. Conclusion

In this study, we present the synthesis of nine new organic push-pull dye sensitizers using pyranilidene fragments, which have been scarcely investigated as potential electron donors in push-pull chromophores so far. The dye electrochemical and light absorption properties were studied and the excited state properties modeled by TD-DFT calculations. These analyses show that all the dyes fulfill the criteria to act as efficient sensitizers for TiO₂ in DSSCs (large Gibbs free energy of the electron injection and dye regeneration, presence of strong charge transfer absorption bands and significant electron density of the LUMO on the anchoring groups). We also found that small structural changes significantly impact the photovoltaic performances, since the PCEs of this series of dyes vary from 1.5% to 5.5% depending on the nature of the substituents on the electron donor group. Together, the measurements of the photovoltaic performances and the IMVS experiment results show that the linker between the pyranilidene and the cyanoacrylic acid plays an important role to optimize these dyes for DSSC applications. The oligothiophene spacer brings π -conjugation, which is favorable to Light Harvesting Efficiency (LHE), but is detrimental to the charge recombination processes. Accordingly, new rod like molecules, such as oligophenylene or ethynylene or fused dithienylene, could be attractive π -conjugated spacer candidates to engineer new push-pull dye sensitizers. All the substituents on the upper part (2 and 6 positions) of the pyranilidene electron donor moiety, except the thienyl group, poorly affect the electronic properties of the resulting dyes and consequently have a limited influence on the photovoltaic performances. The major role of these upper part substituents is most likely to control the packing arrangement of the dyes on the TiO₂ surface. However, a variety of these substituents can be used without affecting the photovoltaic properties of the dyes, since we found that the replacement of a phenyl substituent by a biphenyl or a naphthyl substituent on the 2 and 6 positions of the electron donor group does not significantly change the PCE. On the other

hand, the nature of the substituents on the lower part (substituents on the exocyclic carbon) of the pyranilidene moiety significantly affects the photovoltaic performances of the dyes, since the replacement of a phenyl substituent by a thienyl substituent leads to a noticeable PCE decrease.

This study shows that obtaining an optimal sensitizer dye exhibiting the highest photovoltaic performance requires phenyl substituents being placed in the lower part (substituents on the exocyclic carbon) of the pyranilidene electron donor group, since these groups provide the most suitable dye packing arrangement and allow to control charge recombination reactions. Overall, this study provides a better understanding of the factors controlling the efficiency of these types of dyes and offers some molecular engineering rules to design dyes with improved photovoltaic performances.

Acknowledgments

This research used resources of the GENCI-CINES/IDRIS, of the CCIPL and the Troy cluster, the two latter being installed in Nantes. D.J. is indebted to the *Région des Pays de la Loire*, for continuous support.

References

[1] a) Hagfeldt A, Boschloo G, Sun L, Kloo L, Pettersson H. Dye-Sensitized Solar Cells. *Chem Rev* 2010;110:6595–663; b) Hsu HY, Wang CY, Fathi A, Shiu JW, Chung CC, Shen PS, Guo TF, Chen P, Lee YP, Diao EW G. Femtosecond excitonic relaxation dynamics of perovskite on mesoporous films of Al₂O₃ and NiO nanoparticles. *Angew Chem Int Ed* 2014;53:9339–42.

[2] a) Lewis NS, Nocera DG. Powering the planet: chemical challenges in solar energy utilization. *Proc Natl Acad Sci U.S.A.* 2006;103:15729–35; b) Bandara T, Dissanayake M, Albinsson I, Mellander BE. Dye-sensitized, nano-porous TiO₂ solar cell with poly(acrylonitrile): MgI₂ plasticized electrolyte. *J Power Sources* 2010;195:3730–4.

[3] a) Imahori H, Umeyama T, Ito S. Large π -Aromatic Molecules as Potential Sensitizers for Highly Efficient Dye-Sensitized Solar Cells. *Acc Chem Res* 2009;42:1809–18; b) Wu H P, Ou ZW, Pan TY, Lan CM, Huang WK, Lee HW, Reddy NM, Chen CT, Chao WS, Yeh CY, Diao EWG. Molecular engineering of cocktail co-sensitization for efficient panchromatic porphyrin-sensitized solar cells. *Energy Environ Sci* 2012;5:9843–8; c) Wu YZ, Zhu WH. Organic sensitizers from D- π -A to D-A- π -A: effect of the internal electron-withdrawing units on molecular absorption, energy levels and photovoltaic performances. *Chem Soc Rev* 2013;42:2039–58.

[4] a) O'Regan B, Gratzel M. A low-cost, high-efficiency solar cell based on dye-sensitized colloidal TiO₂ films. *Nature* 1991;353:737–4; b) Higashino T, Imahori H. Porphyrins as excellent dyes for dye-sensitized solar cells: recent developments and insights. Large π -Aromatic Molecules as Potential Sensitizers for Highly Efficient Dye-Sensitized Solar Cells. *Dalton Trans* 2015;44:448–63.

[5] a) Hagfeldt A, Boschloo G, Sun LC, Kloo L, Pettersson H. Dye-sensitized solar cells. *Chem Rev* 2010;110:6595–663; b) Hardin BE, Snaith HJ, McGehee M. The renaissance of dye-sensitized solar cells. *Nature Photonics* 2012;6:162–9.

[6] Freitag M, Teuscher J, Saygili Y, Zhang X, Giordano F, Liska P, Hua J, Zakeeruddin S.M, Moser J-E, Grätzel M, Hagfeldt A. Dye-sensitized solar cells for efficient power generation under ambient lighting. *Nature Photonics* 2017;11:372–9.

[7] a) Ocakoglu K, Harputlu E, Guloglu P, Erten ES. The photovoltaic performance of new ruthenium complexes in DSSC based on nanorod ZnO electrode. *Synth Met.* 2012;162:2125–33; b) Cerda B, Sivakumar R, Paulraj M. Natural dyes as sensitizers to increase the efficiency in sensitized solar cells. *J Phys Conf Ser* 2016;720:012030; c) Argazzi R, Larramona G, Contado C, Bignozzi CA. Preparation and photoelectrochemical characterization of red sensitive osmium complex containing 4,4',4''-tricarboxy-2,2':6',2''-terpyridine and cyanide ligands. *J Photochem Photobiol A Chem* 2004;164:15–21.

[8] a) Lee CW, Lu HP, Lan CM, Huang YL, Liang YR, Yen WN, Liu YC, Lin YS, Diao EWG, Yeh CY. Novel zinc porphyrin sensitizers for dye-sensitized solar cells: synthesis and spectral, electrochemical, and photovoltaic properties. *Chem Eur J* 2009;15:1403–12; b) Bessho T, Constable EC, Graetzel M, Redondo AH, Housecroft CE, Kylberg W, Nazeeruddin MK, Neuburger M, Schaffner S, An element of surprise efficient copper-functionalized dye-sensitized solar cells, *Chem Commun* 2008;0:3717–19.

[9] a) Qu SY, Hua J L, Tian H. Dyes for efficient dye-sensitized solar cells. *Sci China Chem* 2012;55: 677–97; b) Yang JB, Guo FL, Hua J L, Li X, Wu WJ, Qu Y, Tian H. Efficient and stable organic DSSC sensitizers bearing quinacridone and furan moieties as a planar π -spacer. *J Mater Chem* 2012; 22:24356–65; c) Wu YZ, Marszalek M, Zakeeruddin SM, Zhang Q, Tian H, Gratzel M, Zhu WH. High-conversion-efficiency organic dye-sensitized solar cells: molecular engineering on D–A– π -A featured organic indoline dyes. *Energy Environ Sci* 2012;5:8261–72; d) Bessho T, Zakeeruddin SM, Yeh CY, Diau EWG, Gratzel, M. Highly efficient mesoscopic dye-sensitized solar cells based on donor-acceptor-substituted porphyrins. *Angew Chem Int Ed* 2010;49:6646–9; e) Marszalek M, Nagane S, Ichake A, Humphry-Baker R, Paul V, Zakeeruddin SM, Gratzel M. Structural variations of D– π -A dyes influence on the photovoltaic performance of dye-sensitized solar cells. *RSC Adv* 2013;3:7921–7; f) Mao JY, He N N, Ning ZJ, Zhang Q, Guo FL, Chen L, Wu WJ, Hua JL, Tian H. Influence of different electron acceptors in carbazole-based organic sensitizers on the performance of dye-sensitized solar cells. *Angew Chem Int Ed* 2012;51:9873–6.

[10] a) Choi H, Baik C, Kang SO, Ko J, Kang MS, Nazeeruddin MK, Gratzel M. Highly efficient and thermally stable organic sensitizers for solvent-free dye-sensitized solar cells. *Angew Chem Int Ed* 2008;47:327–30; b) Cai N, Li R, Wang Y, Zhang M, Wang P. Organic dye-sensitized solar cells with a cobalt redox couple: influences of π -linker rigidification and dye–bath solvent selection. *Energy Environ Sci* 2013;6:139–47; c) Yao Z, Zhang M, Wu H, Yang L, Li R, Wang P. Donor/Acceptor Indenoperylene Dye for Highly Efficient Organic Dye-Sensitized Solar Cells. *J Am Chem Soc* 2015;137:3799–802.

[11] Wang J, Liu K, Ma L, Zhan X. Triarylamine: versatile platform for organic, dye-sensitized, and perovskite solar cells. *Chem Rev* 2016;116:14675–725.

[12] Liang M, Chen J. Arylamine organic dyes for dye-sensitized solar cells. *Chem Soc Rev* 2013;42:3453–88

[13] a) Yang J, Ganesan P, Teuscher J, Moehl T, Kim YJ, Yi C, et al. Influence of the donor size in D- π -A organic dyes for dye-sensitized solar cells. *J Am Chem Soc* 2014;136:5722–30; b) Alagumalai A, Fairros MKM, Vellimalai P, Chandra Sil M, Nithyanandhan J. Effect of out-of-plane alkyl group's position in dye-sensitized solar cell efficiency: a structure–property relationship utilizing indoline-based unsymmetrical squaraine dyes. *ACS Appl Mater Interfaces* 2016;8:35353–67.

[14] a) Soni SS, Fadadu KB, Vaghasiya JV, Solanki BG, Sonigara KK, Singh A, et al. Improved molecular architecture of D- π -A carbazole dyes: 9% PCE with a cobalt redox shuttle in dye sensitized solar cells. *J Mater Chem A* 2015;3:21664–71; b) Sathiyar G, Sivakumar EKT, Ganesamoorthy R, Thangamuthu R, Sakthivel P. Review of carbazole based conjugated molecules for highly efficient organic solar cell application. *Tetrahedron Lett* 2016;57:243–52.

[15] a) Wan Z, Jia C, Duan Y, Chen X, Li Z, Lin Y. Novel organic sensitizers containing dithiafulvenyl units as additional donors for efficient dye-sensitized solar cells. *RSC Adv* 2014;4:34896–903; b) Luo J, Wan Z, Jia C, Wang Y, Wu X, Yao X. Co-sensitization of dithiafulvenylphenothiazine based organic dyes with N719 for efficient dye-sensitized solar cells. *Electrochim Acta* 2016;211:364–74.

[16] a) Wenger S, Bouit P-A, Chen Q, Teuscher J, Di Censo D, Humphry-Baker R, Moser J-E, Delgado JL, Martín N, Zakeeruddin SM, Grätzel M. Efficient electron transfer and sensitizer regeneration in stable π -extended tetrathiafulvalene-sensitized solar cells. *J Am Chem Soc* 2010;132:5164–9; b) Brunetti FG, López JL, Atienza C, Martín N. π -Extended TTF: a versatile molecule for organic electronics. *J Mater Chem* 2012;22:4188–205.

[17] a) Srinivas K, Yesudas K, Bhanuprakash K, Rao VJ, Giribabu L. Combined experimental and computational investigation of anthracene based sensitizers for DSSC: comparison of cyanoacrylic and malonic acid electron withdrawing groups binding onto the TiO₂ anatase (101) surface. *J Phys Chem C* 2009;113:20117–26; b) Wiberg J, Marinado T, Hagberg DP, Sun L, Hagfeldt A, Albinsson B. Effect of anchoring group on electron injection and recombination dynamics in organic dye-sensitized solar cells. *J Phys Chem C* 2009;113:3881–6.

[18] a) Marco AB, Martínez de Baroja N, Franco S, Garín J, Orduna J, Villacampa B, Revuelto A, Andreu R. Dithienopyrrole as a rigid alternative to the bithiophene π relay in chromophores with second-order nonlinear optical properties. *Chem Asian J* 2015;10:188–97; b) Marco AB, Mayorga Burrezo P, Mosteo L, Franco S, Garín J, Orduna J, Diosdado BE, Villacampa B, López Navarrete JT, Casado T, Andreu R. Polarization, second-order nonlinear optical properties and electrochromism in 4H-pyranylidene chromophores with a quinoid/aromatic thiophene ring bridge. *RSC Adv* 2015;5: 231–42; (c) Marco AB, Andreu R, Franco S, Garín J, Orduna J, Villacampa B, Diosdado BE, López Navarrete J T, Casado T. Push-pull systems bearing a quinoid/aromatic thieno[3,2-b]thiophene moiety: synthesis, ground state polarization and second-order nonlinear properties *Org Biomol Chem* 2013;11: 6338–49; (d) Andreu R, Galán E, Orduna J, Villacampa B, Alicante R, López Navarrete JT,

Casado J, Garín J. Aromatic/Proaromatic Donors in 2-Dicyanomethylenethiazole Merocyanines: From Neutral to Strongly Zwitterionic Nonlinear Optical Chromophores. *Chem – Eur J* 2011;17:826–38.

[19] a) Solanke P, Achelle S, Cabon N, Pytela O, Barsella A, Caro B, Robin-le Guen F, Podlesný J, Klikar M, Bureš F. Proaromatic pyranylidene chalcogen analogues and cyclopenta[c]thiophen-4,6-dione as electron donors and acceptor in efficient charge-transfer chromophores. *Dyes Pigm* 2016;134:129–38; b) Achelle S, Malval JP, Aloïse S, Barsella A, Spangenberg A, Mager L, Akdas-Kilig H, Filaut JL, Caro B, Robin le Guen F. Synthesis, photophysics and nonlinear optical properties of stilbenoid pyrimidine-based dyes bearing methylenepyran donor groups. *ChemPhysChem* 2013; 14, 2725–36; c) Gauthier S, Vologdin N, Achelle S, Barsella A, Caro B, Robin-le Guen F. Methylenepyran based dipolar and quadrupolar dyes: synthesis, electrochemical and photochemical properties. *Tetrahedron* 2013;69: 8392–99; d) Faux N, Robin-le Guen F, le Poul P, Caro B, Nakatani K, Ishow E, Golhen S. Synthesis and NLO Properties of 4-(4H-Chalcogenopyran-4-ylidene and 4H-chalcogenochromen-4-ylidene)-1-(phenylthio)but-2-enylidene Complexes – Electronic Influence of the Carbene Fragment. *Eur J Inorg Chem* 2006; 3489–97.

[20] a) Durand RJ, Gauthier S, Achelle S, Kahlal S, Saillard JY, Barsella A, Wojcik L, Le Poul N, Robin-Le Guen F. Incorporation of a Platinum Center in the Pi-conjugated Core of Push-pull Chromophores for Nonlinear Optics (NLO). *Dalton Trans* 2017;46:3059–69; b) Durand RJ, Gauthier S, Achelle S, Groizard T, Kahlal S, Saillard JY, Barsella A, Le Poul N, Robin-Le Guen F. Push-pull D- π -Ru- π -A chromophores: synthesis and electrochemical, photophysical and secondorder nonlinear optical properties. *Dalton Trans* 2018;47:3965–75; c) Gauthier S, Porter A, Achelle S, Roisnel T, Dorcet V, Barsella A, Le Poul N, Guevara Level P, Jacquemin D, Robin-Le Guen F. Mono- and Diplatinum Polyynediyl Complexes as Potential Push-Pull Chromophores: Synthesis, Characterization, TD-DFT Modeling, and Photophysical and NLO Properties. *Organometallics* 2018; 37:2232–44;

[21] a) Gauthier S, Caro B, Robin-le Guen F, Bhuvanesh N, Gladysz JA, Wojcik L, le Poul N, Planchat A, Pellegrin Y, Blart E, Jacquemin D, Odobel F. Synthesis, photovoltaic performances and TD-DFT modeling of push-pull diacetylide platinum complexes in TiO₂ based dye-sensitized solar cells. *Dalton Trans* 2014;43:11233–42; b) Ferreira E, le Poul P, Cabon N, Caro B, Robin-le Guen F, Pellegrin Y, Planchat A, Odobel F. New D- π -A-conjugated organic sensitizers based on α -pyranylidene donors for dye-sensitized solar cells. *Tetrahedron Lett* 2017;58:995–9. c) Bolag A, Nishida JI, Hara K, Yamashita Y. Enhanced performance of dye-sensitized solar cells with novel 2,6-diphenyl-4H-pyranylidene dyes. *Organic Electronics* 2012;13:425–31. d) Andreu R, Carrasquer L,

Franco S, Garín J, Orduna J, Martínez de Baroja N, Alicante R, Villacampa B, Allain M. 4H-Pyran-4-ylidenes: Strong Proaromatic Donors for Organic Nonlinear Optical Chromophores. *J Org Chem* 2009;74:6647–57.

[22] Marco AB, Martínez de Barojaa N, Andrés-Castána JM, Francoa S, Andreua R, Villacampab B, Ordunaa J, Garín J. Pyranylidene/thienothiophene-based organic sensitizers for dye-sensitized solar cells. *Dyes and Pigments* 2019;161:205–13.

[23] Horiuchi T, Miura H, Uchida S. Highly-efficient metal-free organic dyes for dye sensitized solar cells. *Chem Commun* 2003:3036–7.

[24] Wang P, Klein C, Humphry-Baker R, Zakeeruddin SM, Grätzel M. A high molar extinction coefficient sensitizer for stable dye-sensitized solar cells. *J Am Chem Soc* 2005;127:808–9.

[25] a) Wojcik L, López I, Gauthier S, Cabon N, Le Poul, P, Gloaguen F, Le Poul N. Insights into the radical-radical and radical-substrate dimerization processes for substituted phenylmethylenepyranes. *Electrochimica Acta* 2019;305:304–11; b) Wojcik L, Michaud F, Gauthier S, Cabon N, Le Poul P, Gloaguen F, Le Poul N. Reversible redox switching of chromophoric phenylmethylenepyranes by carbon-carbon bond making/breaking. *J. Org. Chem* 2017;82:12395–405.

[26] Le Bahers T, Adamo C, Ciofini, I. A qualitative index of spatial extent in charge-transfer excitations. *J Chem Theory Comput* 2011;7:2498–506.

[27] Jacquemin D, Le Bahers T, Adamo C, Ciofini, I. What is the “best” atomic charge model to describe through-space charge-transfer excitations ? *Phys Chem Chem Phys* 2012;14:5383–88.

[28] Ciofini ID, Le Bahers T, Adamo C, Odobel, F, Jacquemin D. Through-space charge transfer in rod-like molecules: lessons from theory. *J Phys Chem C* 2012;116:11946–55.

[29] Zhang L, Cole JM. Dye aggregation in dye-sensitized solar cells. *J. Mater. Chem. A*. 2017;5:19541–59.

[30] Clifford, JN, Martínez-Ferrero, E, Palomares E. Dye mediated charge recombination dynamics in nanocrystalline TiO₂ dye sensitized solar cells. *J. Mater. Chem.* 2012;22:2415–22.